Journal of Petroleum Science and Technology 13(2): 38, 2023, Pages 20-28
DOI:10.22078/jpst.2023.5251.1904

Journal of Petroleum Science and Technology
Research Paper
https://jpst.ripi.ir/

The Effect of Cobalt to Iron Ratio on Novel Perovskite Catalysts for Fischer-Tropsch Synthesis

Behnoosh Moshtari[1], Seyed Hasan Hashemabadi[1]* and Yahya Zamani[2]
1 Iran University of Science and Technology, Tehran, Iran
2 Research Institute of Petroleum Industry

Abstract
Fischer-Tropsch synthesis is a direct method to produce fuels with low aromatic and sulfur content. Among various types of catalysts used for Fischer-Tropsch synthesis, the perovskite catalysts are more effective in a wide range of chemical reactions and have significant applications for gas-solid reactions. This study investigates the application of $LaFe_{(1-x)}Co_xO_3$ perovskite catalyst with various Co to Fe ratios in Fischer Tropsch synthesis. The perovskite oxides are prepared via the sol-gel method and characterized using temperature-programmed reduction (H_2-TPR), X-ray diffraction (XRD), Transmission electron micrographs (TEM), and BET surface area techniques. In addition, the catalyst is tested in a fixed bed reactor at 240, 260, 280, and 300 °C and 20 barg pressure. The results show that the crystal structure of $LaFe_{(1-x)}Co_xO_3$ perovskite catalyst is changed and demonstrated high activity due to the iron active site; therefore, by increasing the amount of iron catalyst structure shifts to the orthorhombic and the CO conversion increases noticeably. Results show that the $LaFe0.7Co_{0.3}O_3$ catalyst at 280 °C is a possible candidate for Fischer-Tropes synthesis.

Keywords: Fischer Tropsch Synthesis, Perovskite, Product Selectivity.

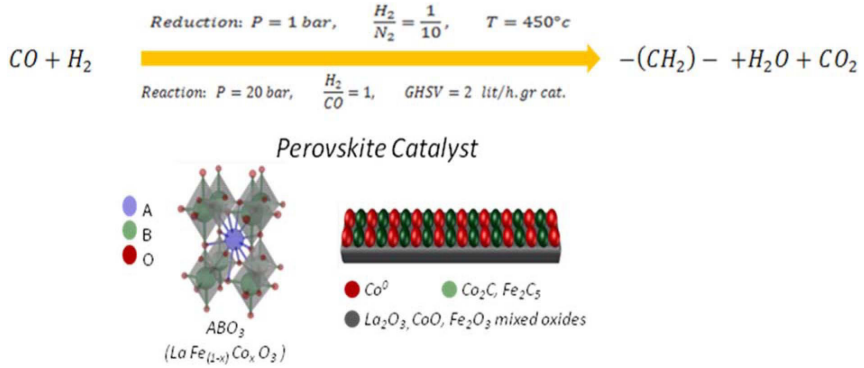

Graphical Abstract

Introduction
Fisher-Tropsh synthesis (FTS) is used to convert syngas to a mixture of hydrocarbons, mainly paraffin and olefins [1, 2]. Due to the availability of immense natural gas resources, producing chemicals such as olefins, aromatics, and oxygenates via the FTS is highly desirable. Many efforts have been made to industrialize the catalysts [3-5]. The hydrocarbon produced using Fischer-Tropsch synthesis is considered clean fuel due to its low sulfur content compared to fossil fuels [6-8]. However, the catalysts in the current process are usually iron and cobalt-based [9]. Cobalt-based catalysts have higher CO conversion, C_5^+ selectivity, and lower WGS (Water gas shift reaction) activity than iron-based catalysts [7-11]. Recently, demands for perovskite catalysts have increased due to their high thermal stability and good performance in all reactions [12-15]. The perovskite catalyst is effective for various chemical reactions [1, 3, 16-21] and has significant applications in gas-solid reactions [16, 17]. In addition, it is efficient for the hydrogenation of alkenes and alkynes and well known for oxidation reactions, including carbon monoxide and

**Corresponding author:* Seyed Hasan Hashemabadi, *Iran University of Science and Technology, Tehran, Iran*
E-mail addresses: drhashemabadi.iust@gmail.com
Received 2023-09-18, Received in revised form 2023-12-09, Accepted 2023-12-26, Available online 2024-02-12

total/partial methane oxidation [1, 2, 14, 18-22]. The general structure of the catalyst is ABO_3, in which A and B are metal groups (A and B are large and small cations, respectively) [23-34]. Due to the stable structure and high matching capacity, various metals with distinct atomic sizes and physicochemical properties can be substituted in the A and B sites [24]. However, the catalyst activity is restricted by the B site, but the thermal stability of the catalyst is determined by the position of A and B cations [35-39].

Although perovskite oxides are ideal catalysts for converting syngas due to their high thermal stability [25-36], the application of the catalysts due to low surface area is limited [38-42]. Moreover, the perovskites depend on the active metals (A and B sites), and the catalyst preparation method has various spatial structures such as triclinic, rhombohedral, tetragonal, orthorhombic, and monoclinic [32].

In the current study, the effect of the Co/Fe ratio in the B site at the La $Fe_{(1-x)}Co_xO_3$ perovskite catalyst has been investigated for Fisher-Tropes synthesis. The catalyst is prepared via the sol-gel method and characterized using XRD, BET, TEM, and H_2-TPR. In addition, the activity of the catalysts for Fischer-Tropsch synthesis was tested in the fixed bed reactor at the temperature and pressure of 240, 260, 280, 300°C, and 20 barg, respectively.

Materials and Methods

Materials

The deionized water was utilized for the synthesis of catalysts. All other materials were utilized in their original form: Iron (III) nitrate ($Fe(NO_3)_3.9H_2O$, Merck, 98%), Cobalt (II) nitrate ($Co(NO_3)_3.6H_2O$, Merck, 99%), Lanthanum(III) nitrate ($La(NO_3)_3.6H_2O$, Merck, 99%), Glycine (NH_2CH_2COOH, Merck, 99%)

Catalyst Preparation

According to the literature, several methods have been reported for synthesizing perovskite catalysts, such as hydrothermal, microwave, precipitation, and sol-gel [11, 43]. In the current research, the perovskite catalysts were prepared using the thermal sol-gel method. In this method, lanthanum, cobalt, and iron salts are solved in deionized water; then glycine is added dropwise and mixed for 2 hours at 80 °C for gel formation [44]. The remaining gel was oven-dried for 4 hours at 180 °C and then calcinated at 550 °C (5°C/min) for 5 hours under the N_2 gas stream.

Catalyst Characterization

XRD: The perovskite catalysts were analyzed using the XRD (Philips PW1729) instrument. The diffraction pattern was obtained using a CuKα lamp with wavelength of λ = 1.542 °A in the angle range 2θ = 1 to 2θ = 80 and step size of 0.06. The particle size was determined based on the XRD information and using the Scherer equation.

BET: The catalyst's surface area, pore volume, and mean pore diameter were measured using the BET (ASAP 3020 Micromeritics) instrument.

H_2-TPR: The Temperature Programmed Reduction (H_2-TPR) test was carried out on the 0.011 g of catalyst, which was heated from 28 to 750 °C (5 °C/min) under a mixture of H_2 and Argon (5% and 95%, respectively) gas with total gas flow rate of 50 Ncc/min using H_2-TPR (Chembet 3000) instrument.

TEM: The Transmission Electron Microscopy (TEM) test was carried out on the catalysts using the TEM (CM120 microscope, Philips) instrument.

Laboratory System

The prepared catalysts were loaded into the reactor accordingly to investigate the catalyst performance in Fischer-Tropsch synthesis.

The setup consists of feeding, reaction, and product separation and analysis.

The general outline of the laboratory system is presented in Fig. 1.

The stainless steel fixed bed reactor had a diameter of 8 mm and a height of 700 mm. The reactor was divided into three equal zones. The lower zone was filled with 2g of a catalyst supported by carborundum both below and above the catalyst till the entrance of the reactor. The reactor temperature is controlled by a furnace with a temperature controller around the reactor.

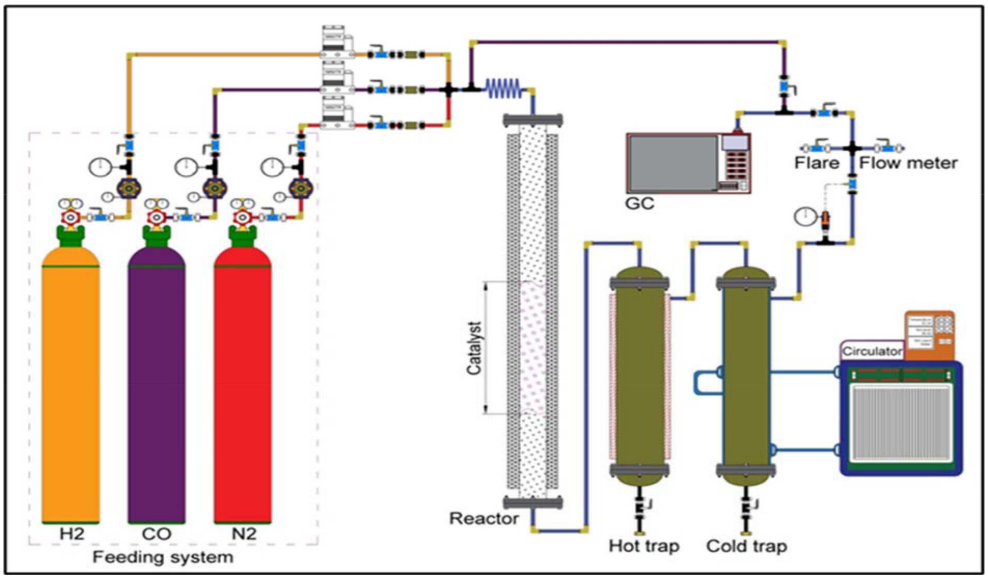

Fig. 1 Laboratory system schematic.

The system is equipped with two traps (hot and cold) to capture light and heavy liquid products to prevent reactor outlet blockage in case of heavy hydrocarbon formation. The feed section is equipped with three mass flow controllers (hydrogen, carbon monoxide, and nitrogen) that let the gases pass and enter toward the catalyst bed. The gases were preheated before entering the catalyst bed. The pressure is adjusted at 20 barg using a pressure valve at the reactor outlet.

Laboratory System

The prepared catalysts were loaded into the reactor accordingly to investigate the catalyst performance in Fischer-Tropsch synthesis.

The setup consists of feeding, reaction, and product separation and analysis.

The general outline of the laboratory system is presented in Fig. 1. The stainless steel fixed bed reactor had a diameter of 8 mm and a height of 700 mm. The reactor was divided into three equal zones. The lower zone was filled with 2g of a catalyst supported by carborundum both below and above the catalyst till the entrance of the reactor. The reactor temperature is controlled by a furnace with a temperature controller around the reactor. The system is equipped with two traps (hot and cold) to capture light and heavy liquid products to prevent reactor outlet blockage in case of heavy hydrocarbon formation. The feed section is equipped with three mass flow controllers (hydrogen, carbon monoxide, and nitrogen) that let the gases pass and enter toward the catalyst bed. The gases were preheated before entering the catalyst bed. The pressure is adjusted at 20 barg using a pressure valve at the reactor outlet.

Afterward, during the reduction process, the mixture of hydrogen and nitrogen gases with a ratio of 1 to 10 (H_2 / N_2 = 1/10), under atmospheric pressure and temperature of 450 °C, passes through the catalyst bed for 24 hours.

Then, the reaction process is executed at various temperatures of 240, 260, 280, and 300 °C, with a constant pressure of 20 bar, while the syngas (H_2/CO=1) is passed through the catalyst bed. In addition, the CO conversion is determined using Equation (1):

$$\%\ \text{conversion of CO} = \frac{\text{moles of CO}_{in}\text{-moles of CO}_{out}}{\text{moles of CO}_{in}} \times 100\% \qquad (1)$$

The liquid products are discharged from the traps in the product separation part, while the gas products are sent to GC (Agilent 7890) via a stainless steel tube. After performing the quantitative analyses of C_1-C_4 hydrocarbons, the C_5^+ hydrocarbons selectivity is defined using Equation (2):

$$S_{C_5^+} = 100 - S_{C_1} + S_{C_2} + S_{C_3} + S_{C_4} + SCO_2 \qquad (2)$$

Results and Discussion

The BET, XRD, TEM, and H_2-TPR tests were carried out on the perovskite to characterize the catalyst properties.

BET Surface

The BET results are represented in Table 1. The results show that under the same calcination conditions, the higher surface area of the catalyst corresponded with higher iron content. Increasing iron content transforms the structure of the perovskite catalyst from rhombohedral to orthorhombic [1]. Furthermore, previous studies on perovskite catalysts have demonstrated that the rhombohedral structure has a lower activity toward CO conversion [1, 24, 28, 45, 46]. Adding iron to the perovskite metal phase decreases the Co concentration, and the catalyst structure shifts to the orthorhombic. The results show that the catalyst surface varies from 9 m^2/g at X=1 to 23 m^2/g at X = 0.3.

Table 1 Specific surface area of La $Fe_{(1-x)}$ Co_x O_3 after calcination at 550 °C.

Sample	SBET (m^2/g)	Pore Volume (cm^3/g)
La CoO_3	9	0.0454
La $Fe_{0.3}Co0.7$ O_3	17	0.0807
La $Fe_{0.5}$ $Co_{0.5}$ O_3	19	0.0852
La $Fe_{0.7}$ $Co_{0.3}$ O_3	23	0.0959

XRD

All the perovskite catalysts were calcinated at 550°C and tested using XRD to define the catalyst's morphology. The XRD diagram of $LaFe_{(1-x)}Co_xO_3$ with various iron content was presented in Figs. 2a-d. The Figs. 2a, b, c, and d correspond with the amount of iron in a catalyst structure. As depicted in Figs.2 a-d, there are two types of crystal structure, depending on iron concentration, determined by the typical diffraction peaks of the perovskite at 2θ and the range between 30-40. Therefore, by increasing the x factor in $LaFe_{(1-x)}Co_xO_3$, the crystal structure transforms from rhombohedral to orthorhombic, which is in line with studies of Bedel et al. and Traversa et al. [1, 47, 48].

$LaFe_{(1-x)}Co_xO_3$ crystal size was calculated according to X-ray diffraction data with Scherer's Equation, and the results are reported in Table 2 [49]:

$$d = \frac{K\lambda}{\beta\cos\theta} \qquad (3)$$

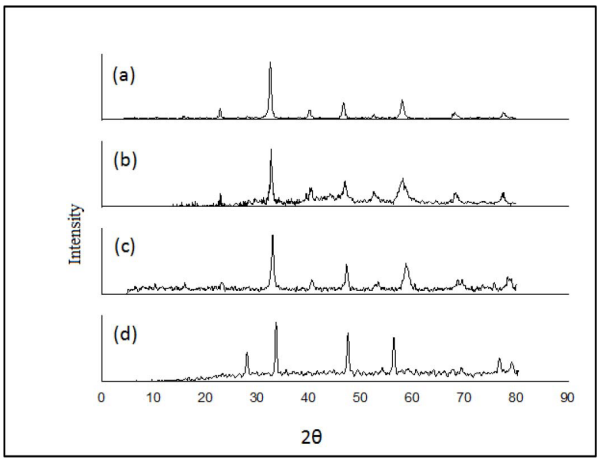

Fig. 2 XRD pattern after calcinations at 550°C: (a) $LaFe0.7Co_{0.3}O_3$, (b) $LaFe_{0.5}$ $Co_{0.5}$ O_3, (c) $LaFe_{0.3}Co_{0.7}$ O_3. (d) $LaCoO_3$.

Table 2 Calculated crystal size with Scherer's Equation.

Sample	Crystal size (nm)
La CoO_3	28.3
La $Fe_{0.3}Co_{0.7}$ O_3	27.1
La $Fe_{0.5}$ $Co_{0.5}$ O_3	24.5
La $Fe_{0.7}$ $Co_{0.3}$ O_3	22.4

TEM

Figs. 3a-d represents catalyst granules' size along with their distribution diagram. TEM result shows a homogeneous distribution of the catalyst grains. The size of grains is in the range of 10-120 nm, and by increasing the amount of iron, the grain's size is increasing accordingly.

H_2-TPR

In the H_2-TPR results presented in Figs. 4a-d, two reduction peaks correspond with the amount of iron in the catalyst structure. The first and second reduction areas are at temperatures around 280 ˚C and 380 to 430 ˚C, respectively. Two sharp peaks in H_2-TPR profiles demonstrate two reducible cations in the B site [24]. The results agree with previous studies [1, 24, 27, 34].

However, the literature confirms that the reduction temperature is greatly influenced by the catalyst's preparation, chemical composition, structure, and morphology [1, 31]. Still, the $LaFe_{(1-x)}Co_xO_3$ reduction properties were affected by the Co/Fe ratio.

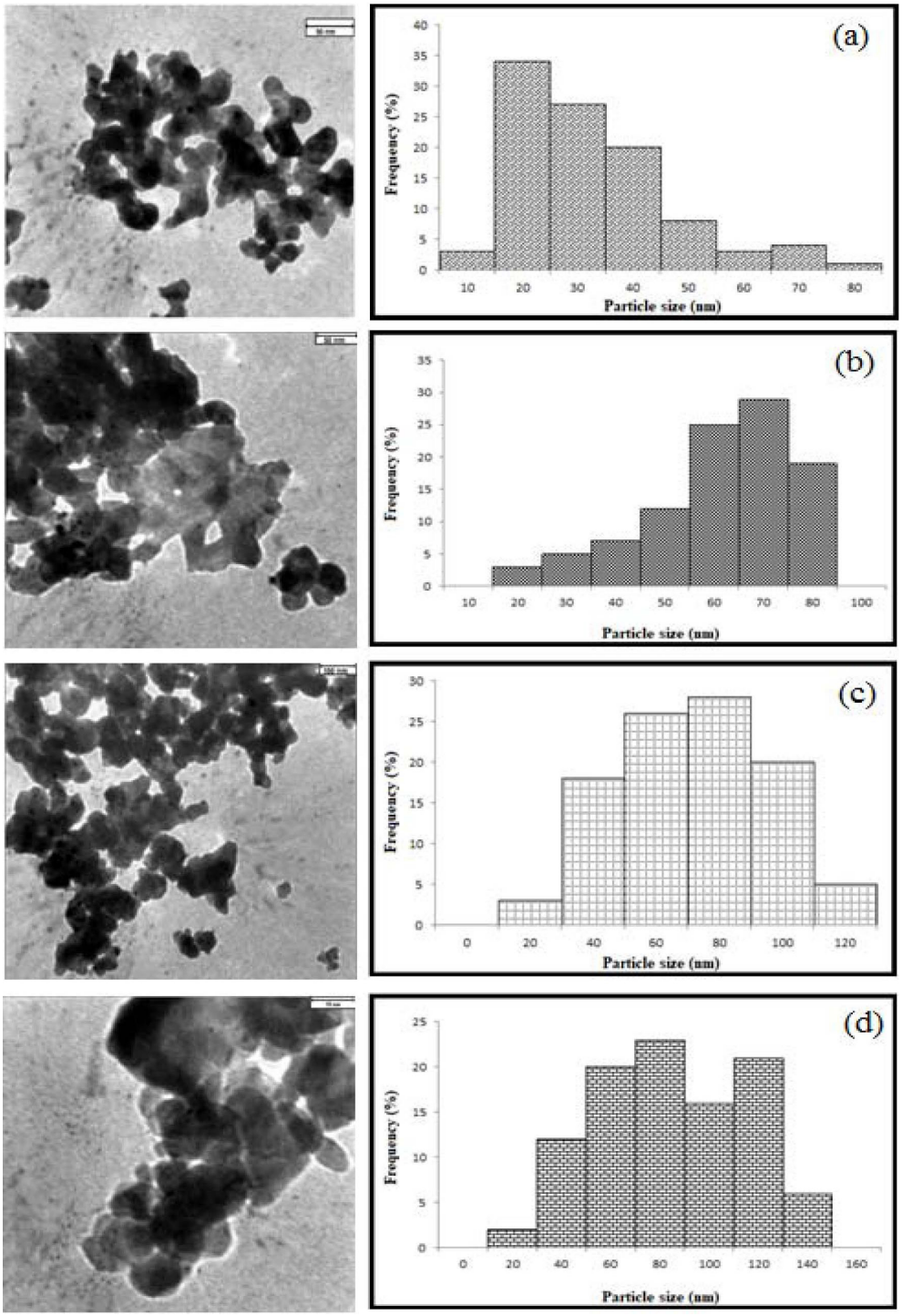

Fig. 3 Transmission electron micrographs: (a) $LaCoO_3$, (b) $LaFe_{0.3}Co_{0.7}O_3$, (c) $LaFe_{0.5}Co_{0.5}O_3$, (d) $LaFe_{0.7}Co_{0.3}O_3$.

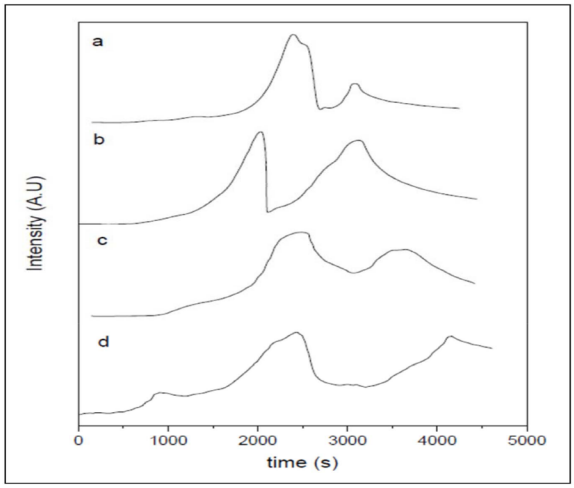

Fig. 4 H_2-TPR profiles perovskite catalysts: (a) $LaCoO_3$, (b) $LaFe_{0.3}Co0.7\ O_3$, (c) $LaFe_{0.5}\ Co_{0.5}\ O_3$, (d) $LaFe_{0.7}Co_{0.3}O_3$.

Moreover, the hydrogen consumption rate is a function of the cobalt amount in the catalyst. The amount of cobalt is presented in Fig. 5. Conversely, the linear increase in hydrogen consumption with X elucidates that the redox cycle of Co is easier to achieve than the Fe redox cycle.

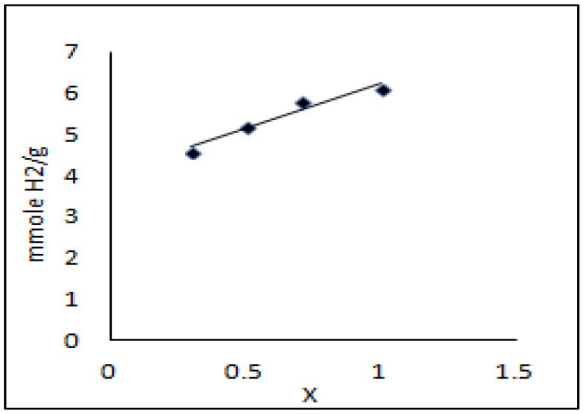

Fig. 5 mmole of H^2/g consume during reduction for $LaFe_{(1-x)}$ Cox O_3.

Fischer-Tropsh Synthesis

The CO conversion is investigated on all catalysts with different amounts of Fe and Co under diverse operating conditions (temperature range of 280-340˚C and the constant pressure of 20 bar). In Fig. 6, the conversion of CO was depicted over different amounts of X. As you can see, a higher CO conversion was achieved when the iron content was high. Therefore, at X = 0.7, a significant amount of CO is reacted, which could be described by structural modification of perovskite from rhombohedral to orthorhombic [1, 29]. In fact, with increasing the amount of iron, the structure of the catalyst changes to the orthorhombic; as a consequence, CO conversion increases accordingly [1, 3]. The conversion of carbon monoxide at different temperatures is presented in Fig. 7. As reported in Fig. 7, CO conversion increases while the temperature increases, which happens for all catalysts. Due to the stable structure of perovskite catalysts, the catalysts are activated at high temperatures; therefore, the CO conversion increases with an increase in temperature. On the other hand, it should be noted that increasing the temperature in the Fischer-Trposch process is not always favorable.

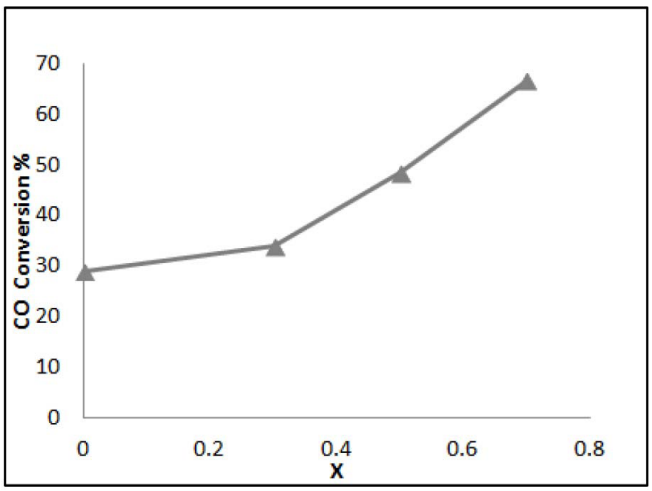

Fig. 6 Effect of Fe on CO conversion at 300°C.

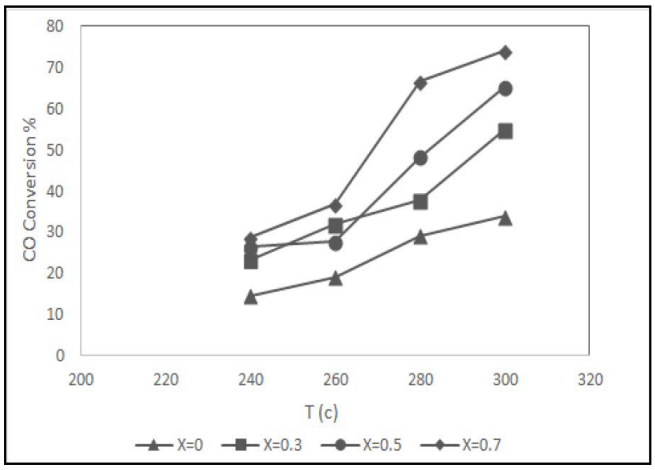

Fig. 7 CO conversion (%) vs. Fischer Tropsch reaction Temperature.

The catalyst's selectivity is a function of temperature, and it was estimated by the amount of CH_4, CO_2, and C_5^+ in the production. The selectivity diagram and yield of C_5^+ products are depicted in Fig. 8 (a,b). It is observed that at a temperature of 240 °C, the catalyst activity is insufficient to produce hydrocarbons, but at a temperature of 300 °C, the selectivity of CH_4 and CO_2 was increased significantly, opposite to C_5^+ was decreased. Therefore, the reaction proceeds towards the light products. It seems the suitable temperature for Fischer-Tropsch synthesis is 280 °C. Furthermore, the selectivity of CH_4 vs. C_5^+ is linear for every four catalysts. It is noted that the linear correlation can be obtained for all perovskite catalysts at the same operating condition [50].

In Fig. 9, the selectivity of CH_4 vs. C_5^+ was depicted for all perovskite catalysts discussed in the current study. In addition, the negative slope of the line indicates that by increasing the CH_4 selectivity, the C_5^+ selectivity was decreased, and the selectivity is not influenced by catalyst characteristics such as crystallite size and pore size. The current results are in agreement with previous studies [51]. Table 3 compares different types of perovskite catalysts concerning selectivity of C_5^+. Among them, the selectivity of $LaFe_{0.7}\ Co_{0.3}\ O_3$ is higher than others, with a value of 39.36%.

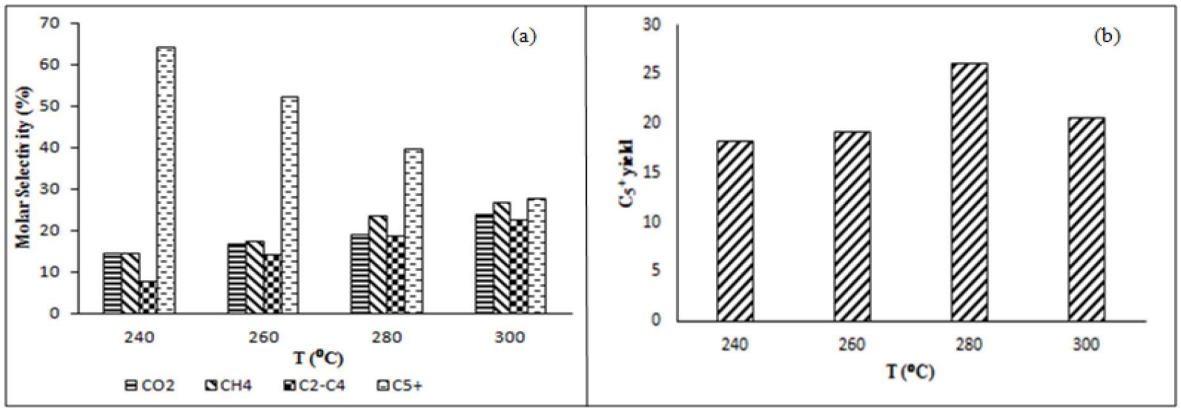

Fig. 8 Fischer-Tropsch (a) product Selectivity (b) C_5^+ yield of $LaFe_{0.7}Co_{0.3}O_3$.

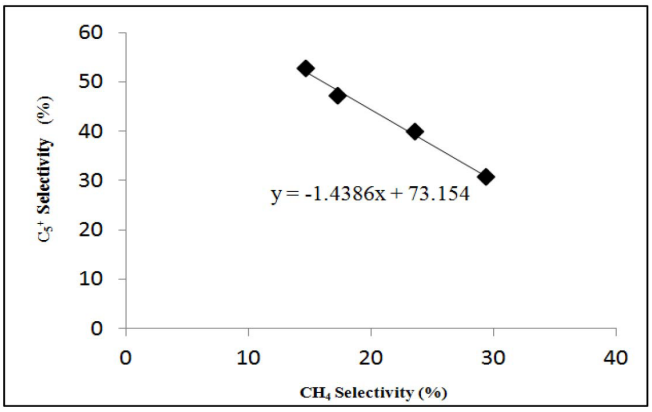

Fig. 9 Relationship between CH_4 and C_5^+ selectivity for perovskite catalysts.

Table 3 The selectivity of literature overview and present work for Fischer-Tropsch synthesis.

catalyst	P (bar)	T (˚C)	H_2/CO	GHSV (1.h-1)	Selectivity (%)	Reference			
					C_1	C_2-C_4	C_5^+	CO_2	
$LaFe_{0.7}Co_{0.3}O_3$	20	280	1	3000	23.5	18.45	39.36	18.69	Present Work
$LaCoO_3$	30	300	2	3500	48.33	23.19	19.02	8.80	[24]
$La_{0.9}Sr_{0.1}CoO_3$	30	300	2	3500	37.5	20.91	29.02	11.8	[24]
$LaFe_{0.6}Co_{0.4}O_3$	10	280	1	3000	52.30	36.20	11.50	24.80	[52]
$LaCoO_3$	67	275	2	5000	48.00	-	-	10.00	[29]

Conclusions

In this study, $LaFe_{(1-x)}Co_xO_3$ perovskite catalyst was evaluated for Fisher_Tropes synthesis. One notable advantage of these catalysts is their robust crystalline structure, which is achieved by incorporating a diverse array of metals within their composition. The catalysts were prepared using the sol-gel method. The results of the XRD analysis demonstrated that as iron content increases, the structure of the catalysts transforms from rhombohedral to orthorhombic, leading to an increasing surface area that is preferable for Fisher-Tropsch synthesis. Adding iron improves the catalyst's performance at high temperatures (above 300°C) significantly; furthermore, adding iron enhances CO conversion and catalyst stability at high temperatures. Although the selectivity of heavy products such as C_5^+ increases, the WGS reaction will prevail, and more CO_2 will be produced. Therefore, due to its high thermal stability and efficient CO conversion, the $LaFe_{0.7}Co_{0.3}O_3$ catalyst at 280 °C is a possible candidate for Fischer-Tropes synthesis.

References

1. Bedel, L., Roger, A. C., Estournes, C., & Kiennemann, A. (2003). Co0 from partial reduction of La (Co, Fe) O_3 perovskites for Fischer–Tropsch synthesis, Catalysis Today, 85(2-4), 207-218, https://doi.org/10.1016/S0920-5861(03)00388-2.
2. Torshizi, H. O., Pour, A. N., Mohammadi, A., & Zamani, Y. (2020). Fischer–Tropsch synthesis using a cobalt catalyst supported on graphitic carbon nitride, New Journal of Chemistry, 44(15), 6053-6062, https://doi.org/10.1039/D0NJ01041C.
3. Lin, X. M., Sorensen, C. M., Klabunde, K. J., & Hadjipanayis, G. C. (1998). Temperature dependence of morphology and magnetic properties of cobalt nanoparticles prepared by an inverse micelle technique, Langmuir, 14(25), 7140-7146, https://doi.org/10.1021/la980509w
4. Arai, H., Yamada, T., Eguchi, K., & Seiyama, T. (1986). Catalytic combustion of methane over various

perovskite-type oxides. Applied catalysis, 26, 265-276, https://doi.org/10.1016/S0166-9834(00)82556-7.
5. Deng, S., Lei, Y., Deng, Y., Lai, Y., & Gao, X. (2022). Recent advances in the application of perovskite catalysts in the dry reforming of methane, Catalysis Research, 2(2), 1-11, doi:10.21926/cr.2202012.
6. Zhang, X., Qian, W., Zhang, H., Sun, Q., & Ying, W. (2018). Online measurement of solids motion in fluidized bed reactor with different distributor for Fischer–Tropsch synthesis, Chinese Journal of Chemical Engineering, 26(10), 2003-2008, doi.org/10.1016/j.cjche.2017.12.003.
7. Li, Z., Si, M., Xin, L., Liu, R., Liu, R., & Lü, J. (2018). Cobalt catalysts for Fischer–Tropsch synthesis: The effect of support, precipitant and pH value. Chinese journal of chemical engineering, 26(4), 747-752, doi.org/10.1016/j.cjche.2017.11.001.
8. Chen, Y., Zhang, J., Jiang, X., Wei, L., Li, Z., & Liu, C. (2020). Nano-ZSM-5 decorated cobalt based catalysts for Fischer-Tropsch synthesis to enhance the gasoline range products selectivity, Journal of the Taiwan Institute of Chemical Engineers, 116, 153-159, doi.org/10.1016/j.jtice.2020.11.007.
9. Li, C. (2018). Modeling and optimization of industrial Fischer–Tropsch synthesis with the slurry bubble column reactor and iron-based catalyst, Chinese Journal of Chemical Engineering, 26(5), 1102-1109, doi.org/10.1016/j.cjche.2018.01.002.
10. Chu, W., Xu, J., Hong, J., Lin, T., & Khodakov, A. (2015). Design of efficient Fischer Tropsch cobalt catalysts via plasma enhancement: Reducibility and performance, Catalysis Today, 256, 41-48, doi.org/10.1016/j.cattod.2015.05.024.
11. Akbari, M., Mirzaei, A. A., Atashi, H., & Arsalanfar, M. (2018). Effect of microemulsion parameters on product selectivity of MgO-supported iron–cobalt–manganese–potassium nanocatalyst for Fischer–Tropsch synthesis using response surface methodology, Journal of the Taiwan Institute of Chemical Engineers, 91, 396-404, doi.org/10.1016/j.jtice.2018.06.004.
12. Tejuca, L. G., & Fierro, J. L. (1992). Properties and applications of perovskite-type oxides, CRC Press, doi.org/10.1201/9781482277258.
13. Wang, Z. J., Yan, Z., Liu, C. J., & Goodman, D. W. (2011). Surface science studies on cobalt Fischer–Tropsch catalysts, ChemCatChem, 3(3), 551-559, doi.org/10.1002/cctc.201000319.
14. Petunchi, J. O., Ulla, M. A., Marcos, J. A., & Lombardo, E. A. (1981). Characterization of hydrogenation active sites on LaCoO3 perovskite, Journal of Catalysis, 70(2), 356-363, doi.org/10.1016/0021-9517(81)90347-X.
15. Bedel, L., Roger, A. C., Rehspringer, J. L., Zimmermann, Y., & Kiennemann, A. (2005). La (1− y) $Co_{0.4}Fe_{0.6}O_3$− δ perovskite oxides as catalysts for Fischer–Tropsch synthesis, Journal of Catalysis, 235(2), 279-294, doi.org/10.1016/j.jcat.2005.07.025.
16. Arandiyan, H., Mofarah, S. S., Sorrell, C. C., Doustkhah, E., Sajjadi, B., Hao, D., & Maschmeyer, T. (2021). Defect engineering of oxide perovskites for catalysis and energy storage: synthesis of chemistry and materials science. Chemical Society Reviews, 50(18), 10116-10211, doi.org/10.1039/D0CS00639D.
17. S Sayadi Borazjani, K., Pouranfard, A., & Razmjooei, S. (2023). Synthesis and Characterization of a New Perovskite Nanocatalyst in CO Hydrogenation, Chemical Engineering & Technology, 46(10), 2110-2119, doi.org/10.1002/ceat.202200272
18. Chan, K. S., Ma, J., Jaenicke, S., Chuah, G. K., & Lee, J. Y. (1994). Catalytic carbon monoxide oxidation over strontium, cerium and copper-substituted lanthanum manganates and cobaltates, Applied Catalysis A: General, 107(2), 201-227, doi.org/10.1016/0926-860X(94)85156-5.
19. Doshi, R., Alcock, C. B., & Carberry, J. J. (1993). Effect of surface area on CO oxidation by the perovskite catalysts La 1− x Sr x MO $_3$-δ (M= Co, Cr). Catalysis letters, 18, 337-343, doi.org/10.1007/BF00765279.
20. Teymouri, M., Bagherzadeh, E., Petit, C., Rehspringer, J. L., Libs, S., & Kiennemann, A. (1995). Reactivity of perovskites on oxidative coupling of methane, Journal of materials Science, 30, 3005-3009, doi.org/10.1007/BF00349675.
21. Wei, L., Chen, J., Lyu, S., Liu, C., Zhao, Y., Zhang, Y., & Li, J. (2021). Isomorphic titanium-substituted mesoporous SBA-16 as support for cobalt Fischer–Tropsch synthesis catalysts: balance between dispersion and reduction. New Journal of Chemistry, 45(31), 13956-13963, doi.org/10.1039/D0NJ04654J.
22. Ichimura, K., Inoue, Y., & Yasumori, I. (1981). Catalysis by mixed oxide perovskites. II. The hydrogenolysis of C_3-C_5 hydrocarbons on $LaCoO_3$, Bulletin of the Chemical Society of Japan, 54(6), 1787-1792, Ichimura, K., Inoue, Y., & Yasumori, I. (1981). Catalysis by mixed oxide perovskites. II. The hydrogenolysis of C_3-C_5 hydrocarbons on $LaCoO_3$, Bulletin of the Chemical Society of Japan, 54(6), 1787-1792.
23. Jacobs, R., Hwang, J., Shao-Horn, Y., & Morgan, D. (2019). Assessing correlations of perovskite catalytic performance with electronic structure descriptors, Chemistry of Materials, 31(3), 785-797, doi.org/10.1021/acs.chemmater.8b03840.
24. Ao, M., Pham, G. H., Sage, V., & Pareek, V. (2016). Structure and activity of strontium substituted $LaCoO_3$ perovskite catalysts for syngas conversion, Journal of Molecular Catalysis A: Chemical, 416, 96-104, doi.org/10.1016/j.molcata.2016.02.020.
25. Bourzutschky, J. B., Homs, N., & Bell, A. T. (1990). Conversion of synthesis gas over LaMn1− xCUx03+ λ perovskites and related copper catalysts, Journal of Catalysis, 124(1), 52-72, doi.org/10.1016/0021-9517(90)90103-Q.
26. Ni, Z., Zhang, X., Bai, J., Wang, Z., Li, X., & Zhang, Y. (2020). Potassium promoted core–shell-structured FeK@ SiO 2-GC catalysts used for Fischer–Tropsch synthesis to olefins without further reduction. New Journal of Chemistry, 44(1), 87-94, doi: 10.1039/c9nj03947c rsc.li/njc.
27. Escalona, N., Fuentealba, S., & Pecchi, G. (2010). Fischer–Tropsch synthesis over LaFe1− xCo_xO_3 perovskites from a simulated biosyngas feed, Applied

Catalysis A: General, 381(1-2), 253-260, doi. org/10.1016/j.apcata.2010.04.022.
28. Tien-Thao, N., Alamdari, H., Zahedi-Niaki, M. H., & Kaliaguine, S. (2006). LaCo1− xCuxO$_3$− δ perovskite catalysts for higher alcohol synthesis, Applied Catalysis A: General, 311, 204-212, doi:.org/10.1016/j. apcata.2006.06.029.
29. Tien-Thao, N., Alamdari, H., & Kaliaguine, S. (2008). Characterization and reactivity of nanoscale La (Co, Cu) O3 perovskite catalyst precursors for CO hydrogenation. Journal of solid state chemistry, 181(8), 2006-2019, doi. org/10.1016/j.jssc.2007.11.016.
30. Tien-Thao, N., Alamdari, H., & Kaliaguine, S. (2008). Characterization and reactivity of nanoscale La (Co, Cu) O3 perovskite catalyst precursors for CO hydrogenation, Journal of solid state chemistry, 181(8), 2006-2019, doi. org/10.1016/j.apcata.2007.04.009.
31. Tien-Thao, N., Zahedi-Niaki, M. H., Alamdari, H., & Kaliaguine, S. (2007). Effect of alkali additives over nanocrystalline Co–Cu-based perovskites as catalysts for higher-alcohol synthesis, Journal of Catalysis, 245(2), 348-357, doi.org/10.1016/j.jcat.2006.10.026.
32. Nguyen, T. T., Zahedi-Niaki, M. H., Alamdari, H., & Kaliaguine, S. (2007). Co-Cu metal alloys from LaCo1-xCuxO$_3$ perovskites as catalysts for higher alcohol synthesis from syngas, International Journal of Chemical Reactor Engineering, 5(1), doi.org/10.2202/1542-6580.1583
33. Fang, Y., Liu, Y., Deng, W., & Liu, J. (2014). Cu-Co bi-metal catalyst prepared by perovskite CuO/LaCoO$_3$ used for higher alcohol synthesis from syngas, Journal of energy chemistry, 23(4), 527-534, doi.org/10.1016/S2095-4956(14)60181-9.
34. Liu, G., Geng, Y., Pan, D., Zhang, Y., Niu, T., & Liu, Y. (2014). Bi-metal Cu–Co from LaCo1− xCuxO$_3$ perovskite supported on zirconia for the synthesis of higher alcohols. Fuel processing technology, 128, 289-296, doi.org/10.1016/j.fuproc.2014.07.010.
35. Lee, Y. N., Lago, R. M., Fierro, J. L. G., & González, J. (2001). Hydrogen peroxide decomposition over Ln1−$_x$A$_x$MnO$_3$ (Ln= La or Nd and A= K or Sr) perovskites. Applied Catalysis A: General, 215(1-2), 245-256, doi. org/10.1016/S0926-860X(01)00536-1.
36. Van Roosmalen, J. A. M., Cordfunke, E. H. P., Helmholdt, R. B., & Zandbergen, H. W. (1994). The defect chemistry of LaMnO$_{3\pm\delta}$: 2. Structural aspects of LaMnO$_{3+\delta}$, Journal of Solid State Chemistry, 110(1), 100-105, doi.org/10.1006/jssc.1994.1141.
37. Sis, L. B., Wirtz, G. P., & Sorenson, S. C. (1973). Structure and properties of reduced LaCoO$_3$, Journal of Applied Physics, 44(12), 5553-5559, doi.org/10.1063/1.1662195.
38. Keav, S., Matam, S. K., Ferri, D., & Weidenkaff, A. (2014). Structured perovskite-based catalysts and their application as three-way catalytic converters—A Review. Catalysts, 4(3), 226-255, doi.org/10.3390/catal4030226.
39. Panich, N. M., Pirogova, G. N., Korosteleva, R. I., & Voronin, Y. V. (1999). Oxidation of CO and hydrocarbons over perovskite-type complex oxides, Russian chemical Bulletin, 48, 694-697.
40. Thao, N. T. (2013). Synthesis of Co-Cu/La$_2$O$_3$ Pervoskites for Hydrogenation of CO, Asian Journal of Chemistry, 25(14), 8082, doi.org/10.14233/ajchem.2013.15120.
41. Zhang, Q., & Saito, F. (2000). Mechanochemical synthesis of LaMnO3 from La$_2$O$_3$ and Mn$_2$O$_3$ powders, Journal of Alloys and Compounds, 297(1-2), 99-103, doi.org/10.1016/S0925-8388(99)00606-4.
42. Ramaswamy, V., Awati, P., & Tyagi, A. K. (2004). Lattice thermal expansion of LaCo1− $_x$Cu$_x$O$_3$, Journal of alloys and Compounds, 364(1-2), 180-185, doi.org/10.1016/S0925-8388(03)00496-1.
43. Liu, Z., Chen, W. F., Zhang, X., Zhang, J., Koshy, P., & Sorrell, C. C. (2019). Structural and microstructural effects of Mo$_3$+/Mo$_5^+$ codoping on properties and photocatalytic performance of nanostructured TiO$_2$ Thin films, The Journal of Physical Chemistry C, 123(18), 11781-11790, doi.org/10.1021/acs.jpcc.9b02667.
44. Mohammadi, M. R., Cordero-Cabrera, M. C., Ghorbani, M., & Fray, D. J. (2006). Synthesis of high surface area nanocrystalline anatase-TiO$_2$ powders derived from particulate sol-gel route by tailoring processing parameters, Journal of Sol-gel Science and Technology, 40, 15-23, doi.org/10.1007/s10971-006-8267-0.
45. Rodriguez, G., Bedel, L., Roger, A. C., Udron, L., Carballo, L., & Kiennemann, A. (2003). Dry Reforming of Ethane on Trimetallic Perovskites LaCoxFe1-xO$_3$: Characterizations and Reactivity, doiI:10.1021/bk-2003-0852.ch004.
46. Zhu, Q., Cheng, H., Zou, X., Lu X., Xu Q. & Zhou Zh. (2015). Synthesis, characterization, and catalytic performance of La0. 6Sr0. 4NixCo1–xO$_3$ perovskite catalysts in dry reforming of coke oven gas, Chinese Journal of Catalysis, 36(7): 915-924, doi.org/10.1016/S1872-2067(14)60303-X.
47. Traversa, E., Nunziante, P., Sakamoto, M., Sadaoka, Y., & Montanari, R. (1998). Synthesis and structural characterization of trimetallic perovskite-type oxides, LaFexCo1− xO$_3$, by the thermal decomposition of cyano complexes, La [FexCo1− x (CN$_6$)]· nH$_2$O, Materials Research Bulletin, 33(5), 673-681, doi.org/10.1016/S0025-5408(98)00044-0.
48. Traversa, E., Nunziante, P., Sakamoto, M., Sadaoka, Y., & Montanari, R. (1998). Synthesis and structural characterization of trimetallic perovskite-type oxides, LaFexCo1− xO3, by the thermal decomposition of cyano complexes, La [FexCo1− x (CN$_6$)]· nH$_2$O, Materials Research Bulletin, 33(5), 673-681, doi.org/10.1016/j.jechem.2021.08.023.
49. Monshi, A., Foroughi, M. R., & Monshi, M. R. (2012). Modified Scherrer equation to estimate more accurately nano-crystallite size using XRD, World journal of Nano Science and Engineering, 2(3), 154-160, 154-160, doi: 10.4236/wjnse.2012.23020.
50. Lögdberg, S., Lualdi, M., Järås, S., Walmsley, J. C., Blekkan, E. A., Rytter, E., & Holmen, A. (2010). On the selectivity of cobalt-based Fischer–Tropsch catalysts: Evidence for a common precursor for methane and long-chain hydrocarbons, Journal of Catalysis, 274(1), 84-98, doi.org/10.1016/j.jcat.2010.06.007.
51. Rytter, E., Tsakoumis, N. E., & Holmen, A. (2016).

On the selectivity to higher hydrocarbons in Co-based Fischer–Tropsch synthesis. Catalysis Today, 261, 3-16, doi.org/10.1016/j.cattod.2015.09.020

52. Bedel, L., Roger, A. C., Rehspringer, J. L., & Kiennemann, A. (2004). Structure-controlled La-Co-Fe perovskite precursors for higher C_2-C_4 olefins selectivity in Fischer-Tropsch synthesis, In Studies in surface science and catalysis, 147, 319-324, Elsevier, doi. org/10.1016/S0167-2991(04)80071-5.